PNAS RESEARCH ARTICLE | NEUROSCIENCE APPLIED MATHEMATICS

Finger stability in precision grips

Neelima Sharma[a] and Madhusudhan Venkadesan[a,1]

Edited by Peter Strick, University of Pittsburgh Brain Institute, Pittsburgh, PA; received December 22, 2021; accepted February 7, 2022

Stable precision grips using the fingertips are a cornerstone of human hand dexterity. However, our fingers become unstable sometimes and snap into a hyperextended posture. This is because multilink mechanisms like our fingers can buckle under tip forces. Suppressing this instability is crucial for hand dexterity, but how the neuromuscular system does so is unknown. Here we show that people rely on the stiffness from muscle contraction for finger stability. We measured buckling time constants of 50 ms or less during maximal force application with the index finger—quicker than feedback latencies—which suggests that muscle-induced stiffness may underlie stability. However, a biomechanical model of the finger predicts that muscle-induced stiffness cannot stabilize at maximal force unless we add springs to stiffen the joints or people reduce their force to enable cocontraction. We tested this prediction in 38 volunteers. Upon adding stiffness, maximal force increased by 34 ± 3%, and muscle electromyography readings were 21 ± 3% higher for the finger flexors (mean ± SE). Muscle recordings and mathematical modeling show that adding stiffness offloads the demand for muscle cocontraction, thus freeing up muscle capacity for fingertip force. Hence, people refrain from applying truly maximal force unless an external stabilizing stiffness allows their muscles to apply higher force without losing stability. But more stiffness is not always better. Stiff fingers would affect the ability to adapt passively to complex object geometries and precisely regulate force. Thus, our results show how hand function arises from neurally tuned muscle stiffness that balances finger stability with compliance.

precision grip | stability | human hand | cocontraction | muscle elasticity

Significance

Hand skills rely on the precision grip to hold objects with the fingertips. In rare instances, our finger's joints undergo a form of buckling when we push with the fingertip and snap into hyperextension. Suppressing this instability is crucial for hand use, but how the nervous system avoids buckling is unknown. We studied people applying forces with the tip of their index fingers and found that the nervous system relies on the spring-like action of muscles for stability. The muscles cocontract to stabilize the joints but reduce the strength and compliance of our fingers. Thus, the motor skill of precision grip arises from the careful control of muscle cocontraction to balance the trade-off between finger stability, strength, and flexibility.

Precision grip, as the name implies, is the precise and stable application of fingertip forces. In this grip style, the fingers are relatively stationary while the fingertips exert force (1). Stable precision grips played a key role in the evolution of human hand dexterity (2–5). But the inherent mechanics of multilink chains make the fingers prone to many types of instabilities when the fingertip experiences forces (6, 7). The nervous system often masks these instabilities by using a lifetime of learned control strategies. Therefore, we rarely witness them in everyday experience. Understanding how the nervous system suppresses these instabilities is needed to explain hand function, or its loss due to disease or aging.

Instabilities that arise when pushing on surfaces can be categorized as those affecting the tip where the force is applied (6–11), or the internal degrees of freedom associated with posture (12–14). Tip instabilities are particularly severe when a stiff finger or limb makes contact with a rigid surface (6). When feedback control is used to precisely apply tip forces, the fingertip's position may become unstable and start to oscillate, which also destabilizes the applied force (6, 8). One strategy is to increase the compliance of the finger or limb (15–18). Such stiffness control and its generalization to impedance control in dynamic contexts (6) have proven quite effective in controlling contacts in robots.

Postural stability of the internal degrees of freedom has received considerably lesser attention than tip stability, and has only been studied in models (12, 13) or robots (14). Kinematic chains with many internal degrees of freedom are prone to buckle and lose postural stability under external compressive forces (*SI Appendix*, sections 1A and 1B), analogous to the buckling of slender columns. Consider pushing a rigid surface with the index fingertip (Fig. 1), and focus on the mechanics within the plane of the finger. In this setting, the index finger has three internal degrees of freedom between the knuckle and the tip. When the tip does not slip, it is subject to two translational constraints within the finger's plane. Thus the finger is kinematically underdetermined by one degree. It is this degree of freedom that could become unstable.

To suppress postural instabilities, humans appear to use a conflicting strategy to that of stable force feedback control, namely, to make the limb stiffer. Potential instabilities of finger or limb posture when applying contact force have not been studied much, but a related behavior of stabilizing the posture of a handheld tool has been investigated previously (11). Rancourt and Hogan (11) show that, when using a tool like a handheld drill, more force applied on the wall made the orientation of the drill more susceptible to

Author affiliations: [a]Department of Mechanical Engineering & Materials Science, Yale University, New Haven, CT 06520

Author contributions: N.S. and M.V. designed research, performed research, contributed new reagents/analytic tools, analyzed data, and wrote the paper.

The authors declare no competing interest.

This article is a PNAS Direct Submission.

[1]To whom correspondence may be addressed. Email: m.venkadesan@yale.edu.

This article contains supporting information online at https://www.pnas.org/lookup/suppl/doi:10.1073/pnas.2122903119/-/DCSupplemental.

Published March 16, 2022.

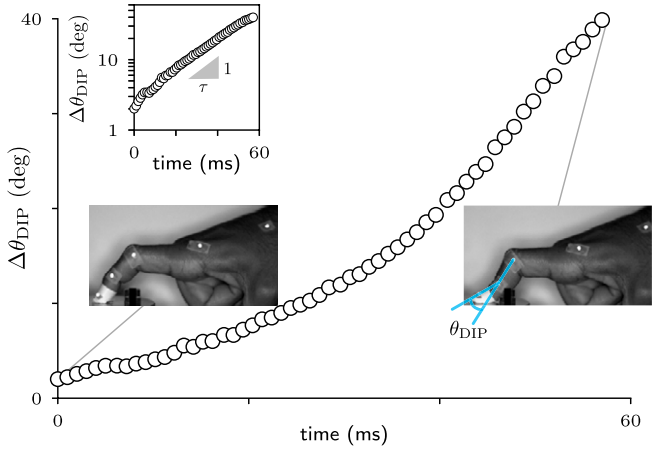

Fig. 1. Buckling of the index finger joints. Sample trial showing the change in the angle of the DIP, $\Delta\theta_{DIP}$. Every fifth sample is plotted for clarity (black circles). (*Top Inset*) Linear log plot of the exponential growth in DIP angle. The time constant τ for the unstable growth in $\Delta\theta_{DIP}$ is found using the slope. For this trial, $\tau = 20$ ms. (*Bottom Insets*) Snapshots of the index finger at the beginning and the end of the sample trial.

becoming unstable, and that hand stiffness is critical for stabilizing the drill. The nervous system uses stiffening as a strategy for postural stability in other contexts as well, such as dealing with unstable environmental dynamics when moving the arm (19) or the destabilizing effects of motor noise (20). Higher stiffness, which is harmful for tip stability under force feedback control, may be what stabilizes the internal degrees of freedom of our fingers and limbs. But the role of stiffness remains debated and unresolved in several contexts involving postural stability. Examples include standing in humans (13, 21), horses (22), and cats (12), as well as arm (20) and finger movements (23). We presently lack studies to tease apart the role of stiffness versus other strategies such as feedback control for maintaining postural stability during contact.

In this paper, we investigate postural stability of our fingers during maximal force application, by using the index finger as a representative example. Occasionally, people use a hyperextended posture when gripping objects, such as when holding a pen. However, when large fingertip forces are applied in a hyperextended posture, load-supporting tissues such as tendons and volar plates could suffer injuries, as occurs in climbing sports (24–26). Furthermore, when it comes to precise manipulation and forceful grasping, people generally use a flexed posture (3–5, 27). Therefore, this paper investigates finger stability in flexed postures. Our approach is inspired by the study of Rancourt and Hogan (11), who used maximal force tasks to probe the neural strategy that stabilizes the posture of a handheld drill. The central idea is to challenge the nervous system by making the internal mechanical response as unstable as possible. Because buckling-type instabilities are generally more severe at higher forces, our study examines how the fingertip's maximal force is affected by external modifications to the finger that alter stability. Moreover, the muscle activation pattern that people use at submaximal fingertip force is a linearly scaled version of the pattern they use at maximal force (23, 28, 29). Thus, understanding stability at maximal force may also help us understand the properties at submaximal forces. In a series of experimental and mathematical studies, we show that people rely on cocontraction and the spring-like properties of the muscles to prevent the finger from buckling, and that the maximal fingertip force they can exert is limited by stability rather than strength.

Results

Postural Instability of the Index Finger. We first conducted a study with nine volunteers to assess the severity of the buckling instability in the index finger (see *Materials and Methods*). They were instructed to apply the largest normal force possible on a rigid surface, with no explicit instruction about stability. We asked them to repeatedly try to push harder until we recorded 33 instances of postural instabilities. The instability manifested as a sudden change in the finger's posture where one of the three finger joints ended up in a hyperextended angle. The distal interphalangeal joint (DIP) buckled most frequently, in 28 out of 33 instances that we captured (Fig. 1 and Movie S1), so we used the DIP angle to analyze the temporal characteristics of the buckling event. The DIP joint angle grew exponentially ($R^2 > 0.9$) with a time constant smaller than 45 ms in 19 out of 28 trials, and never exceeded 80 ms (Fig. 1 and *SI Appendix*, Table S3).

The nerve conduction latency for the round trip from the hand to the spinal cord exceeds 45 ms, and the fastest sensory-driven finger response is usually timed at 65 ms or more (30). Such long latencies would make it challenging to stabilize the finger using neural feedback control. We cannot rule out feedback control solely on the basis of comparison of timescales, but the rapid growth of the instability implies that feedback-driven strategies would suffer from a lack of robustness to sensory noise. Yet the finger was stable for most of the trials; 40 out of 63 trials were stable in seven subjects, and the number of nonbuckling events was not recorded for the other two subjects. This led us to postulate that the open-loop strategy of muscle cocontraction and the joint stiffness it induces is used to stabilize the finger. Muscles are intrinsically stiffer when producing more force, a property known as short-range stiffness (31, 32). Therefore, the harder someone pushes with the fingertip, the higher the muscle and overall finger stiffness (33) (*SI Appendix*, section 1A). So, stability could just be a byproduct of the muscles contracting to produce force. Alternatively, the need to remain stable may constrain the maximum exertion of fingertip force. We performed additional analyses and experiments to find out whether stability is a byproduct or a constraint.

Stability at Maximal Force. We investigated postural stability using a previously developed detailed anatomical model of the index finger (34, 35) (*SI Appendix*, section 1A). The finger was modeled as a three-link, planar kinematic chain, and driven by seven muscles (Fig. 2*A*). The tip was constrained to not translate to capture the absence of fingertip slip, but could freely rotate (35). Muscle activations were specified by a normalized seven-dimensional (7D) vector $\vec{a}$ with values between zero and one, which governs both muscle force and stiffness (12, 32) (*SI Appendix*, section 1A). Activating the muscles drives the finger's joints with torques $\vec{\tau}$, applies a fingertip force $\vec{f}$, and induces stiffness K at the joints.

The planar finger model has only one unconstrained degree of freedom. Therefore, the constrained dynamics of the finger are defined by a projection of the finger's dynamics onto the null space of the constraints that are imposed on the fingertip (*SI Appendix*, section 1A). The orthonormal basis vectors of the null space are expressed as columns of the null space matrix P, which, in the case of the single degree of freedom finger, reduces to a single null space vector. Thus, the 3×3 stiffness matrix K associated with the multilink finger reduces to a scalar stiffness $k_{joint} = P^T K P$ when projected onto the finger's unconstrained degree of freedom. In the absence of feedback control, stability requires the

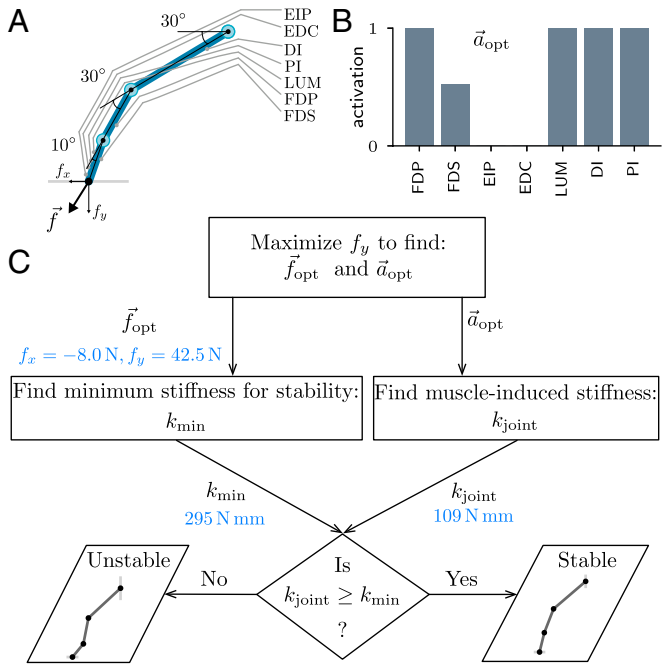

Fig. 2. Modeling study to test whether stability is a byproduct of fingertip force. (*A*) Schematic of a planar model of the index finger that maintains contact at the fingertip and is driven by seven muscles. All seven muscles attach to locations in the hand and arm that are proximal to the MCP joint. (*B*) The optimal activation pattern $\vec{a}_{\text{opt}}$ that maximizes the vertical component of the fingertip force at a fixed posture $\vec{\theta} = (30°, 30°, 10°)$. This is the posture used in subsequent experiments in this paper. (*C*) The decision tree to test whether muscle-induced stiffness leads to stability when the activation pattern is chosen solely to maximize fingertip force. The computed force and stiffnesses at $\vec{\theta} = (30°, 30°, 10°)$ are in blue. The finger is unstable at the maximal force because $k_{\text{joint}} < k_{\text{min}}$.

muscle-induced joint stiffness k_{joint} to exceed a minimum threshold k_{min} that depends on the tip force (*SI Appendix*, section 1B),

$$k_{\text{joint}} > k_{\text{min}} \text{ for stability.} \quad [1]$$

We computed the optimal muscle activation pattern $\vec{a}_{\text{opt}}$ that maximized the vertical force without any constraints imposed on stability (Fig. 2*B* and *SI Appendix*, section 1C). This activation produces a tip force $\vec{f}_{\text{opt}}$ and joint stiffness k_{joint} because of muscle's short-range stiffness. This stiffness k_{joint} was compared with the minimum stiffness k_{min} needed for stability at the maximal force $\vec{f}_{\text{opt}}$ (Fig. 2*C* and *SI Appendix*, section 1B). For the same posture as the experiments $(30°, 30°, 10°)$, we found $k_{\text{joint}} = 109$ N mm and $k_{\text{min}} = 295$ N mm. Thus, the finger is unstable for the activation pattern that maximizes tip force (Fig. 2). We also found that all possible postures that do not hyperextend the joints while maintaining the same tip position as $(30°, 30°, 10°)$ are unstable at the maximal force (*SI Appendix*, Fig. S1). Therefore, stability does not automatically arise as a byproduct of force application.

Once the finger becomes unstable, the posture grows along the unstable mode specified by the null space vector P. For the posture $(30°, 30°, 10°)$, the null space vector is $\text{P} = (0.06 \quad -0.49 \quad 0.87)^{\text{T}}$. Because the DIP component is the largest in magnitude, we expect the DIP joint to manifest the largest joint angle change when the finger buckles. This prediction is consistent with the numerical simulation of the nonlinear equations of the finger model (*SI Appendix*, section 1D and Movie S2), and the recorded buckling events in human subjects. The metacarpophalangeal (MCP) or the proximal interphalangeal (PIP) joint buckled only rarely during our experiments (*SI Appendix*, Table S3), consistent with the smaller MCP and PIP components of the null space vector P.

The results support the hypothesis that stability rather than muscular capacity constrains the maximal voluntary fingertip force. A limitation of the model is that it does not include the series compliance of the tendons. However, that would only decrease the overall stiffness, making it less feasible for the finger to remain stable. The result of the model that stability cannot arise unless the muscle contraction is explicitly planned for that purpose would therefore remain true even if tendons were considered. Therefore, we predict that people should be able to produce more force if their finger is externally stiffened to reduce or eliminate the postural instability. We tested this prediction in experiments with volunteers.

Effect of Externally Stiffening the Finger. We instructed 39 consenting volunteers to stably apply the largest force they could with their index fingertip against a rigid surface (one subject was excluded because of experimental issues [*Materials and Methods*]). To test the prediction of the model, we compared the maximal force of a free index finger with trials where we externally stiffened the finger by attaching a custom-molded thermoplastic splint. Motivated by the large DIP component of the unstable mode, we used two splint designs (Fig. 3*A*): one that stiffened the DIP and the PIP joints (2J splint) and another that only stiffened the PIP joint (1J splint). Because the finger has only one net degree of freedom, both splint designs would stiffen the finger, with lesser stiffness induced by the 1J splint. We recorded, smoothed, and processed the fingertip force and surface electromyograms (EMG) of the flexor digitorum profundus (FDP) and flexor digitorum superficialis (FDS) from all 38 subjects and additionally recorded EMG of the extensor digitorum communis (EDC) in a subset of 16 subjects. The maximal force F_{max} is the maximum of the force trace that was smoothed using a 1-s window. The normalized maximal force f_{max} is the maximal force normalized by the maximal force from all the trials of a given subject. The flexor EMG measure $\text{EMG}_{\text{flexors}}$ is a physiological cross-sectional area (PCSA)-weighted average of the rms of the filtered and maximum voluntary contraction (MVC)-normalized EMG from the two flexors during the 1-s window where force was maximized (*Materials and Methods* and Fig. 3*B*).

Presence of a splint significantly affected the normalized maximal force f_{max} ($F_{2,263} = 144.57$, $p < 0.0001$), and $\text{EMG}_{\text{flexors}}$ ($F_{2,263} = 40.22$, $p < 0.0001$). The 38 subjects consisted of two subsets: a subset of 16 subjects with randomized order of splint conditions (free finger before splinted finger for 7 out of 16 subjects), and a second subset where the splinted trials were after the free finger so that fatigue associated with maximal force trials does not bias the results toward showing a force increase with the splint. For the subset with randomized order of splint conditions, the trial order did not have a significant effect on the difference in normalized force for either splint condition (one-joint: $F_{1,14} = 3.24$, $p = 0.09$, two-joint: $F_{1,14} = 0.41$, $p = 0.53$). In the complete dataset with 38 subjects, trial order (free or splinted first) did not have a significant effect on f_{max} or $\text{EMG}_{\text{flexors}}$ ($F_{1,218} = 2.13$, $p = 0.15$ and $F_{1,190} = 0.46$, $p = 0.49$, respectively). There was also no significant interaction between splint condition and the order of presentation of the trials on either f_{max} or $\text{EMG}_{\text{flexors}}$ ($F_{2,68} = 2.28$, $p = 0.11$ and $F_{2,69} = 2.36$, $p = 0.10$, respectively).

Relative to the free finger, the normalized maximal force significantly increased for the two-joint and one-joint conditions by $\Delta f_{\text{max}} = 0.34 \pm 0.03$ and 0.23 ± 0.03, respectively (mean $\pm$ SE; Fig. 3*C*; $p < 0.0001$ in both conditions). There was subject-to-subject variability in the magnitude of increase, but the force

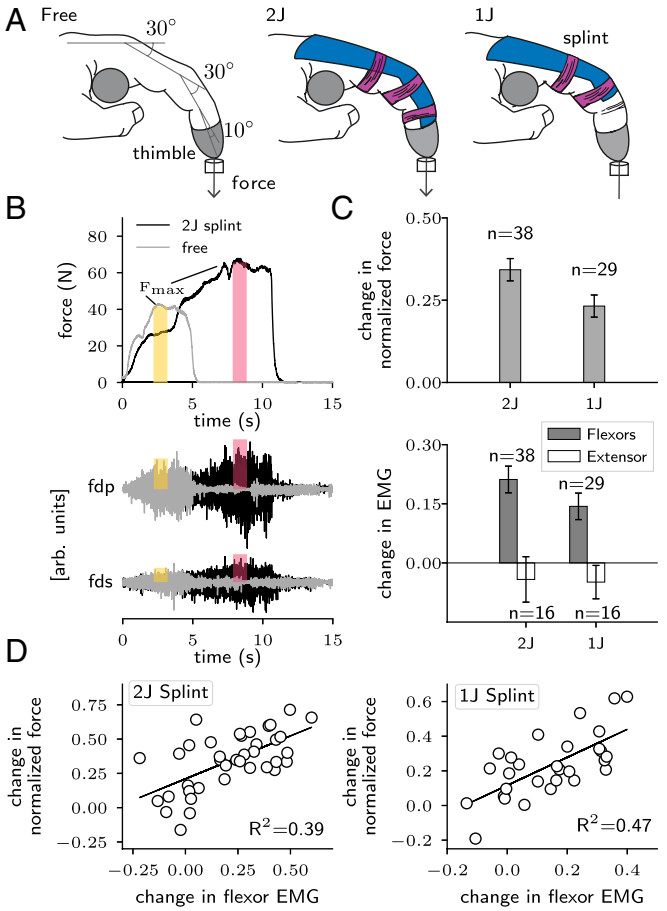

Fig. 3. Maximal force upon stiffening the finger. (*A*) Three conditions were tested at the posture (30°, 30°, 10°): no splint (free), two-joint split (2J), or one-joint splint (1J). (*B*) For a sample subject, the shaded rectangles show the time window when the maximal force occurred, pink for 2J and yellow for free, which are overlaid on the vertical force and raw EMG recordings from FDP and FDS. EMG rectangles are scaled 6× for clarity, but the force rectangles are to scale. (*C*) Change due to the 2J and 1J splints, relative to the free finger, in the maximal normalized force f_{max}, flexor EMG, and extensor EMG. The bars and whiskers show the mean and SE, respectively. (*D*) Scatter plots and regression fits of the change in EMG versus change in force between the splint and the free conditions, for the 2J and 1J conditions.

increased for all but three subjects with the two-joint splint, and for all but one with the one-joint splint. EMG from flexors also significantly increased for the two-joint ($p = 0.04$) and one-joint ($p = 0.04$) conditions, by $\Delta EMG_{flexors} = 0.21 \pm 0.03$ and 0.14 ± 0.03, respectively (mean ± SE; Fig. 3*C*). Statistically significant differences were not found between the two splint types for either normalized force or EMG from flexors.

The increases in normalized force Δf_{max} and normalized flexor EMG $\Delta EMG_{flexors}$ were significantly correlated with each other for both the two-joint (R^2 = 0.39, $p < 0.0001$) and one-joint (R^2 =0.47, $p < 0.0001$) conditions, despite the generally noisy nature of surface EMG measurements, showing that the increased tip force was because of higher muscle activity (Fig. 3*D*). Detailed statistics and verification of assumptions are provided in *SI Appendix*.

We conclude that the nervous system refrains from producing truly maximal force with an unsupported finger. Upon stiffening the finger, especially the DIP joint in the two-joint splint, the maximal force increased. This is consistent with the prediction that, once stability is no longer a concern, a higher force can be applied. The increase in flexor EMG activity with force indicates that the nervous system could tap into additional muscle force capacity, but only when the finger was externally stabilized. We performed an analysis of cocontraction to understand how the splint affords additional muscle force capacity and to probe the origin of intersubject variability.

Cocontraction and Maximal Force. The idea behind more force with the splint is that the splint provides stiffness for stability, thus allowing muscle cocontraction to decrease, which, in turn, allows for more muscle contribution to tip force. To analyze changes in cocontraction with the splint, we recorded surface EMG from the extrinsic extensor EDC in a subset of 16 subjects, in addition to the extrinsic flexors FDP and FDS. Force and EMG were normalized per subject by the respective largest recorded value, and the aggregate $EMG_{flexors}$ was estimated. The extensor and flexors are approximate antagonists, implying that lesser cocontraction would manifest as a reduction in the ratio $EMG_{EDC}/EMG_{flexors}$ upon adding the splint. A one-way ANOVA with finger condition (free, 1J, or 2J) as the factor and the ratio $EMG_{EDC}/EMG_{flexors}$ as the dependent variable was significant ($F_{2,45} = 3.80$, $p = 0.03$). Post hoc contrasts showed that the ratio was significantly smaller for the 2J splint ($p = 0.049$, Δratio $= -0.43$) and borderline for the 1J splint ($p = 0.06$, Δratio $= -0.42$) compared with the free finger (Fig. 4*A* and *SI Appendix*, Table S10).

However, the finger's muscles are not organized as a simple uniarticular agonist–antagonist system. Therefore, producing joint torques to apply fingertip force in a specific direction leads to coactivation of even seemingly antagonistic muscles (34), and produces joint stiffness as a byproduct (Fig. 2*B*). To account for these complexities and refine the cocontraction analysis, we reason that the total EMG has two portions: one that contributes to fingertip force with stiffness as a byproduct and another that lies in the null space of the mapping from muscle contraction to fingertip force. The null space component contributes solely to joint stiffness but not the fingertip force, and we term it cocontraction. We hypothesize that force increases upon adding the splint because a smaller null space component would suffice for stability. Therefore, if the splint reduced the cocontraction component, the same force could be produced with lesser EMG; that is, the ratio of EMG to force would be lesser with the splint (hypothesis schematic in Fig. 4*B*). One-way ANOVA with finger condition as the factor and the EMG to force ratio as the dependent variable was significant for all three muscles (FDS: $F_{2,45} = 4.29$, $p = 0.02$; FDP: $F_{2,45} = 3.69$, $p = 0.03$; EDC: $F_{2,45} = 9.79$, $p = 0.0003$; Fig. 4*C*). Post hoc contrasts showed that the 2J splint always led to a significant decrease in the EMG to force ratio, but the 1J splint led to a significant ratio decrease only for the EDC (*SI Appendix*, Table S11). As seen from the optimization for maximizing tip force (Fig. 2*B*), the EDC has a nil or weak projection onto the tip force for the posture used in our study. So EDC activity is probably most strongly associated with finger stiffening, which is consistent with the result that EMG_{EDC} was most sensitive to adding a splint, 1J or 2J, and responded by nearly halving in magnitude.

The cocontraction analysis could also help us understand the interindividual differences in force increase with the splint. It is possible that not all subjects increased their force output by the same relative magnitude when the splint was added, because of individual differences in the extent of reduction in cocontraction. We hypothesize that stiffening the finger using a splint allows reduced cocontraction, thus resulting in a force gain. To assess this, we extended the analysis of EMG to force ratio to assess how well the decrease in EDC cocontraction could explain the change in maximal voluntary force. The EDC is chosen as the primary muscle for the analysis because of its more direct role in finger stiffness and minimal or nil contribution to fingertip force.

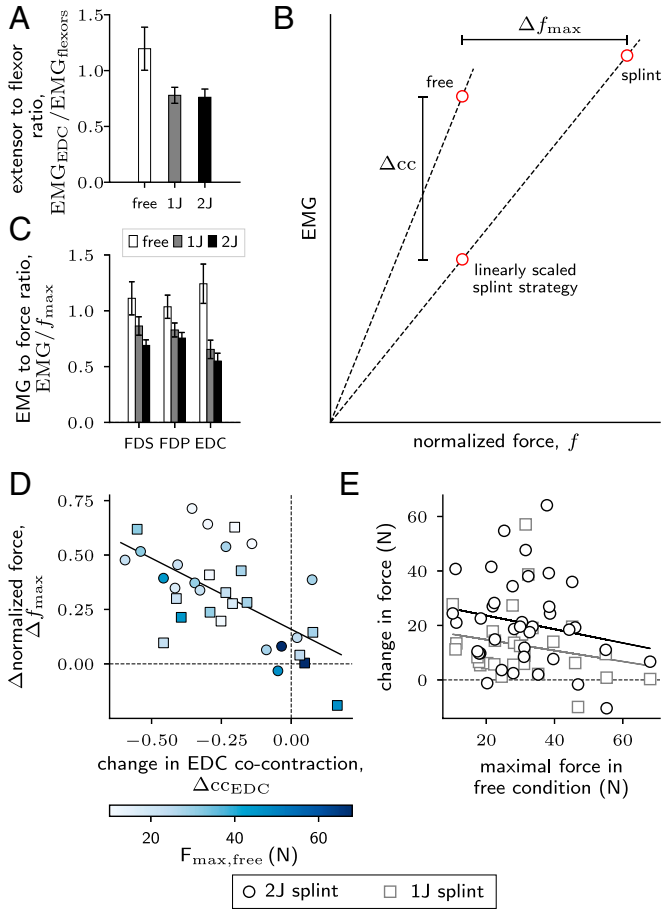

Fig. 4. Cocontraction and maximal force. (*A*) Ratio of extensor to flexor activity for the free, 1J, and 2J splint conditions (n = 16). For *A* and *C*, the bars and whiskers show the mean and SE, respectively. (*B*) Pictorial demonstration of the hypothesis that the free finger is more cocontracted relative to the splinted condition, as seen by a steeper slope for the free finger compared to the splint condition in the normalized EMG–force space. (*C*) EMG to normalized force ratios for the flexors FDS and FDP, and the extensor EDC, for the free, 1J, and 2J splint conditions (n = 16). (*D*) Scatter plot and regression fit of the change in EDC cocontraction versus the change in normalized force. The scatter plot is colored by the magnitude of the free finger's baseline force (n = 16). (*E*) Scatter plot and regression fits of the free finger's baseline force versus the change in force between the splinted and the free conditions for the 2J (black, n = 38) and the 1J (gray, n = 29) splints.

To compare EDC cocontraction while also accounting for overall differences in fingertip force magnitude, we used the finding from previous studies that people linearly scale their EMG patterns as they vary their force (23, 28, 29). Thus, by using the ratio of forces between splinted and free conditions as a scaling factor, the excess EDC cocontraction Δcc_{EDC} was defined as the difference in EMG between the linearly scaled splinted trial and the free trial (Fig. 4*B*),

$$\Delta cc_{EDC} = EMG_{EDC,\,splint}\frac{f_{max,free}}{f_{max,splint}} - EMG_{EDC,\,free}. \quad [2]$$

Lesser cocontraction implies a negative Δcc_{EDC}. A linear regression, with the change in normalized force Δf_{max} as the dependent variable and Δcc_{EDC} as the regressor, showed significant correlation between cocontraction change and force change ($F_{1,30} = 16.93$, $p = 0.0003$, $R^2 = 0.36$, slope $\pm$ SE= -0.65 ± 0.16, intercept $\pm$ SE= 0.15 ± 0.05; Fig. 4*D*). We also tested an alternative hypothesis that the force gain with the splint is minimal or zero in some subjects because they are not limited by stability to begin with and would exhibit high force capabilities even without the splint. A regression of the nonnormalized force increase due to the splint versus the nonnormalized force under free conditions was not significant for either the 2J or 1J splints (2J: $F_{1,36} = 1.48$, $p = 0.23$; 1J: $F_{1,27} = 1.34$, $p = 0.26$; Fig. 4*E*). Furthermore, the change in cocontraction Δcc_{EDC} was not significantly correlated with the free finger's maximal force ($F_{1,30} = 3.31$, $p = 0.08$), thus making it unlikely that differences in cocontraction reduction were simply because some subjects were strong to begin with.

Interindividual variability in cocontraction reduction with the splint may reflect differences in the exploration of new areas of muscle contraction space, perhaps because the splinted trials are unlike normal experience. The baseline force was unable to explain the force difference showing that people who are strong to begin with could still produce more force with the splint, so long as they decreased their cocontraction. Future studies could refine our results and probe learning and neuromotor exploration of the feasible space of strategies by using intramuscular readings from all seven muscles.

Submaximal Forces. The trade-off between cocontraction and maximal force suggests that, at submaximal forces, the muscles may have the leeway to cocontract and modulate stiffness without affecting force. To investigate this, we used the finger model and numerically found activation patterns with minimum and maximum joint stiffness k_{joint} when applying a submaximal force ("1" and "4" in Fig. 5*A*; *SI Appendix*, section 1E; posture: $30°, 30°, 10°$). Both these patterns produce the same horizontal force as the maximal solution (Fig. 2*B*) but just 9 N of force

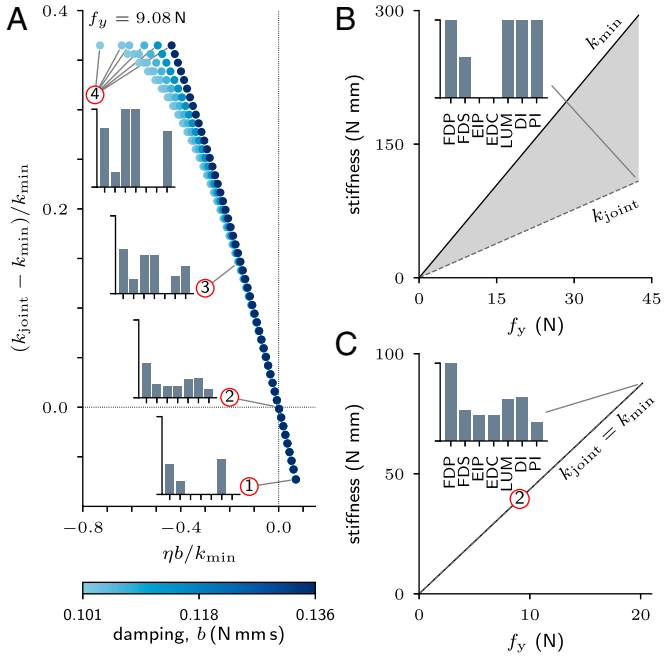

Fig. 5. Muscle cocontraction, stiffness, and stability at submaximal force. (*A*) Monte Carlo simulations densely sampled the 4D space of activation patterns, all of which produce the same tip force but vary in stiffness and stability ($f_y = 9.1$ N, $f_x = -8.0$ N). Using the nondimensional variables $\eta b/k_{min}$ and $(k_{joint} - k_{min})/k_{min}$ for stability and stiffness, respectively, the 4D space of activations collapses into a family of 1D curves that are parametrized by the damping value. Near the origin, the 1D stability–stiffness curves merge into a universal line with slope $= -1$ according to the asymptotic relation given in Eq. **3**. (*B*) The unstable optimal activation $\vec{a}_{opt}$ (*Inset*) that maximizes tip force, and (*C*) the marginally stable pattern "2" are linearly scaled to vary the tip force. The joint stiffness k_{joint} and the minimum stiffness k_{min} also scale linearly, thus preserving the stability properties of the original activation pattern. (*Inset*) Maximally scaled up version of pattern "2." Posture for all plots: $(30°, 30°, 10°)$.

vertically, which is 4.68× lower than maximal. Because the force is submaximal, there is a 4D null space for the mapping from muscle activations to fingertip force. All the null space activation patterns apply the same joint torques and tip forces, but their stiffness varies between those of "1" and "4" in Fig. 5*A*, and they have different eigenvalues η. The eigenvalue η governs stability and depends on the stiffness and damping that are induced by muscle contraction, and the finger's mass (*SI Appendix*, section 1B and Eq. **S1.11**). Unlike short-range stiffness models for muscle, we presently lack accurate models for the damping induced by muscle contraction (36). But stability does not depend on damping and only depends on the sign of the real part of the eigenvalue, that is, on the stiffness deficit $k_{\text{joint}} - k_{\text{min}}$ (*SI Appendix*, section 1B).

We sampled the null space using 6 × 100 million Monte Carlo simulations at six different damping values b (*SI Appendix*, section 1E), and show the results on a nondimensional stability–stiffness space (Fig. 5*A*). Although damping does not affect stability, we explored different values to show the behavior away from marginal stability. We chose damping values so that the finger is critically damped or overdamped, like past measurements (33). Through asymptotic analysis of the eigenvalue near the point of marginal stability when $k_{\text{joint}} = k_{\text{min}}$, we derived nondimensional variables for the relevant eigenvalue and stiffness (*SI Appendix*, section 1B and Eq. **S1.11**). The minimal stiffness for stability is given by $k_{\text{min}} = f_0\ell$, where f_0 is the tip force magnitude and ℓ is a posture-dependent length scale (*SI Appendix*, section 1A). As k_{joint} nears k_{min}, the stability-dominating eigenvalue η that has the most positive real part is asymptotically given by

$$\eta b/k_{\text{min}} \approx -(k_{\text{joint}} - k_{\text{min}})/k_{\text{min}}. \quad [3]$$

This trade-off between stability $\eta b/k_{\text{min}}$ and stiffness $(k_{\text{joint}} - k_{\text{min}})/k_{\text{min}}$ is a universal (asymptotic) relationship that is independent of the finger's mass, and accounts for differences in damping, posture, force magnitude, or force direction.

Within the null space are stable patterns like "3" (*SI Appendix*, section 1E and Movie S2) and marginally stable patterns like "2" in Fig. 5*A* with stable and unstable patterns on either side of them. Importantly, as the cocontraction decreases and the finger approaches marginal stability, the nondimensional stability–stiffness curves collapse onto a universal line with slope $= -1$ given by Eq. **3**. Thus, more cocontraction improves stability but also makes the finger stiffer.

We used the model to examine stability when a specific activation pattern is linearly scaled, in turn, linearly scaling the tip force. This is motivated by simultaneous intramuscular EMG recordings from all seven muscles in humans (23, 28, 29), which showed that people exert submaximal forces by linearly scaling the maximal force activation pattern. The tip force, the contraction-induced joint stiffness, and the minimum stiffness needed for stability scale linearly with the activation pattern (*SI Appendix*, sections 1A and 1B). Therefore, producing submaximal forces by scaling the maximal force pattern $\vec{a}_{\text{opt}}$ does not help stability, and the finger remains unstable (Fig. 5*B*). However, for the marginally stable activation pattern "2" in Fig. 5*A* that produces submaximal force, the marginal stability is preserved whether the activations are scaled up or down (Fig. 5*C*).

Discussion

We have shown that fingers are prone to buckle under tip forces, because of which the maximum exertion of fingertip force is limited by stability rather than muscular capacity. The experimentally measured time constants of the buckling instability suggest that people may have to rely on cocontraction-induced stiffness because feedback control may not be robust. Indeed, people significantly cocontracted their finger muscles when producing fingertip forces, likely for stability. Although muscle's short-range stiffness is proportional to force, it does not automatically guarantee stability. Only select combinations of muscle contraction and cocontraction patterns can help stiffen and stabilize the finger. Our cocontraction analyses, using EMG and a finger model, show that stiffness due to muscle-induced cocontraction is a viable stabilizing strategy only at submaximal forces. Thus, even when instructed to maximize force, people apply lesser force than their muscle strength would allow.

Muscle's stiffness and open-loop stability of contacts are important not only for maximal force production but also for precision grips using lighter forces. If a specific activation pattern lends stability at maximal force, any linear scaling of that pattern will preserve stability. This understanding helps interpret past experimental measurements that, when instructed to vary their fingertip force magnitude, people linearly scaled the muscle activation pattern that they used for maximal stable voluntary force (23, 28, 29). Such linear scaling of the maximal pattern may simply reflect stability preservation. We have shown that stability at maximal voluntary force is likely because of muscle-induced stiffness. When people use scaled versions of the stable maximal voluntary pattern, the finger would continue to remain stable. Therefore, we infer that people rely on muscle's short-range stiffness for stability when using precisions grips with light forces.

Although neural feedback control may not be a robust strategy to prevent buckling at maximal force, it might still be effective at lighter forces. This is because the real part of the eigenvalue that governs the rate of growth of instabilities could be smaller at lighter forces. For a pattern $\vec{a} = \alpha\vec{a}_0$ that scales an unstable pattern $\vec{a}_0$ by a factor $\alpha < 1$, the original eigenvalue η_0 becomes $\eta = \alpha\eta_0(b_0/b)$, where b_0 and b are the damping associated with the original and scaled patterns, respectively. How damping scales with muscle contraction is presently unclear, but it is hypothesized to scale nonlinearly with activation (33, 36), so the eigenvalue would vary with the scaling factor α. Based on the estimate that the fingertip is substantially overdamped at low forces (33), the unstable growth of the finger's posture is quite likely slower at lower activations. A high force that was outside the ability of feedback control to stabilize could thus become stabilizable at lower activation levels. But stability is still a key objective for selecting coordination patterns that allow feedback to augment the role of muscle's stiffness. Future studies are needed to test whether neural feedback is used in this manner, or whether people rely mostly on open-loop stability based on muscle's stiffness even when applying light fingertip forces.

In contrast to our finding that people relied on cocontraction to stabilize the finger's internal degrees of freedom at maximal force, previous studies on endpoint force and position control find that neural feedback was the dominant factor (37–40). One difference from our study is that these past studies investigated low forces, where feedback may prove effective. Our results show that using neural feedback to stabilize the finger at maximal forces may not be robust under sensory noise because the time constant for the buckling instability is smaller than feedback latency. At lower forces, rapid reflexes and other slower sensorimotor feedback may complement the role of muscle cocontraction, but studies focused on sensory systems are needed to investigate these issues. Nevertheless, sensory feedback from the tip force is likely involved in our experiments, as evinced by the fact that the subjects knew to limit their forces to not buckle.

More stiffness is better for postural stability but has implications for everyday hand usage. Although people preshape their hand to match the object about to be gripped (41), the fingers need to further deform upon contact to adapt to the object's precise geometry (42). Compliance is essential for the fingers to deform and adapt the grasp to the object's geometry (16, 18, 43, 44), and is also needed to avoid the well-known instabilities associated with tip under force feedback control (6, 8). But the compliance for adaptive grasping has to be traded off against stiffness for postural stability. More work is needed to understand this trade-off, but the augmentation of open-loop stability by neural feedback at light forces may help manage the trade-off. The universal stability–stiffness curve shows how some patterns may be weakly unstable and allow the finger to be more compliant than strictly enforcing open-loop stability. Thus, our findings on the stability–stiffness trade-off may underlie the selection of strategies for stable yet compliant grasps. Open questions also remain on how such strategic muscle cocontraction is acquired through experiential learning, and how these patterns are related to the vigorously debated neuromuscular synergies (45–47). Nevertheless, the generality of our results implies that muscle's role in open-loop stabilization must be considered.

Our results and analyses present some possible generalizations and implications for other areas. MVC measurement in clinical functional testing, and in neuromechanical and biomechanical studies (48, 49), is influenced by stability and should employ means to delineate the role of stability versus muscular capacity in maximal EMG and force production, perhaps by externally providing stability. Our results translate to settings beyond the index finger. Because inertia is not involved in the universal nondimensional stability–stiffness curve at the margin of stability, our results are applicable to multilink chains of diverse length scales. Simulation studies have found that contact-induced postural instabilities could occur in the legs of standing cats, humans, and horses (12, 13, 22). As animal limbs typically have more muscles than kinematic degrees of freedom, joint stiffness can be controlled independent of the torques, and cocontraction could be used to maintain stability (12, 22). In robotic limbs also, stiffness and torques can be independently controlled, because variable impedance actuators are increasingly prevalent (50). Our results are applicable even when the condition of a rigid tip contact is relaxed to include a compliant contact, such as during multifingered grasps. The proportionality between the minimum joint stiffness for stability and tip force is an intrinsic property of multilink chains such as the finger. Similar stability considerations would apply to all the fingers involved in the grasp, and the grip force would be limited by the finger most prone to buckle. Therefore, our findings apply broadly across animals and machines for achieving compliant, adaptive, and open-loop stable contacts, and specifically help us understand how finger stability affects the control of precision grips.

Materials and Methods

We conducted two separate experiments with the voluntary participation of right-handed adults who had no history of hand injuries or impairments: 1) experiment 1 to record finger buckling: $n = 10$, 7 males (M), 3 females (F), age 24 y to 47 y; and 2) experiment 2 to test maximal force with splints: $n = 39$, 26M, 13F, age 18 y to 47 y.

Subjects studied the consent form, and the experimenter discussed potential risks of the study and their option to withdraw from the study at any time. The experiment was performed after informed consent from the subjects, and in accordance with the relevant guidelines and regulations. The detailed procedures for seeking informed consent were approved by Yale University's institutional review board (HIC# 2000029475). A similar procedure was followed for the study conducted in India, with approval from the Institute Ethics Committee (Human Studies) of the National Centre for Biological Sciences, Bengaluru, India. One subject from experiment 1 was excluded because they never exhibited buckling events, which was the goal of the study. One subject from experiment 2 was excluded because their finger repeatedly buckled and did not yield reliable data.

Experiment 1: Buckling Timescale. Subjects maintained a flexed index finger posture of their choosing, with the fingertip pushing on a horizontal steel plate (Fig. 1). They were asked to maximize the distal fingertip force while maintaining a flexed finger posture with no regard for postural stability. Circular 3-mm reflective markers were attached to the radial aspect of the MCP, PIP, and DIP joints, the fingertip, and the second metacarpal's proximal end. A high-speed camera (Photron FASTCAM Mini AX100, MEC) recorded the instances of buckling in the lateral (radial) view of the index finger at 4,500 frames per second (fps) for subject 1 and 5,000 fps for rest of the subjects. Trials were separated by 2 min to reduce fatigue.

We estimated the change in the joint angles $\Delta\theta_x$, where x is either DIP, PIP, or MCP, from the videos using custom software. The time history $\Delta\theta_x(t)$ was used once the angle increased past 2°, and until the subject-dependent end of buckling (*SI Appendix*, Table S3). To estimate the time constant τ for the hypothesized exponential growth $\Delta\theta_x(t) = \Delta\theta_0 e^{t/\tau}$, we performed a linear regression of $\log \Delta\theta_x(t)$ versus t using the middle half of the data to avoid end effects associated with the log transform. The slope of the semilog plot is equal to $1/\tau$ (Fig. 1, *Top Inset*). The estimated time constants and R^2 of the fits are reported for the 33 trials where the finger buckled (*SI Appendix*, Table S3). MATLAB (version 9.8.0.1323502) was used for the image and regression analyses.

Experiment 2: Splinted Finger. The second experiment tested the model's predictions by measuring the change in maximal voluntary force when the stability of the finger was altered by externally stiffening it.

Experimental apparatus. Subjects wrapped their thumb and unused fingers of the right hand around a ground-mounted nonslip handle and pushed on a horizontal steel plate with their index finger. The handle was adjusted so that the MCP, PIP, and DIP joints were at 30°, 30°, and 10° flexion, respectively (Fig. 3*A*). Using established methods (23, 29, 34), the fingertip was covered by a subject-specific custom-molded thermoplastic thimble (Turbocast®, T-Tape Company) and fixed using Vetrap bandage (3M) to yield a well-defined contact point and consistent friction.

To stiffen the finger, we attached subject-specific thermoplastic two-joint and one-joint splints to the dorsal face of the index finger using Vetrap bandage. The splints were molded to each subject's finger at the posture (30°, 30°, 10°). The two-joint splint covered MCP, PIP, and DIP joints and stiffened the PIP and DIP joints, but the one-joint splint covered only the MCP and PIP joints, and stiffened the PIP joint.

Experimental protocol. The subjects were asked to try two to six times to apply the greatest vertical force they could during the measurement window without letting the finger buckle or the tip slip on the surface, with at least 2 min rest between tries. Three finger conditions were tested: free, two-joint splint (2J), and one-joint splint (1J). For nine subjects (set A), we tested free and 2J fingers with a 15-s measurement window. For 14 subjects (set B), the free, 1J, and 2J fingers were measured using a 20-s window. For 16 subjects (set C), the free, 1J, and 2J fingers were measured using a 15-s window. To control for motor learning, the order was randomized in set A (free before splint for seven subjects) and set C (free before splint for seven subjects). To control for fatigue, the free finger was always first in set B. Subjects were acclimatized to the splint by handling objects and lightly pushing on surfaces before measurement. The vertical fingertip force was displayed as a live trace on a monitor. The fingertip never slipped, but trials where the free finger buckled were excluded.

Data collection. Fingertip force was recorded at 2,000 Hz by rigidly fixing a six-axis load cell (model 45E15A4-M63J-EF, JR3 Inc.) between the steel plate and a rigid bench. Surface EMG was acquired at 2,000 Hz using wireless electrodes (Trigno Wireless EMG System, Delsys Inc.). We palpated the ventral side of the forearm when the subject resisted forces on the index finger, to identify the two extrinsic flexors, FDP and FDS, and attached the electrodes to the skin over the muscle belly using hypoallergenic double-sided tape and Vetrap bandage.

For set C, additional EMG was recorded from one extensor, EDC. We verified the electrode placement by asking subjects to push the experimenter's hand using their index finger, while observing the EMG traces.

Signal processing. EMG recordings were band-stop filtered in the range 48 Hz to 52 Hz and 98 Hz to 102 Hz with zero phase distortion to remove electrical noise for sets A and B (India uses a 50-Hz AC supply), and in the range 58 Hz to 62 Hz and 118 Hz to 122 Hz for set C (United States uses a 60-Hz AC supply). We then high-pass filtered at 20 Hz to remove movement artifacts, full-wave rectified, and passed through a fourth-order Butterworth filter with a time constant of 0.23 s to adjust for the muscle's excitation–contraction dynamics (29).

The force and the processed EMG were moving average filtered with a 1-s window (Fig. 3*B*) to find the maximal voluntary force F_{max} and the EMG at that time. The fingertip force vector across trials was oriented 5.0 $\pm$ 2.8 degrees (mean $\pm$ SD) from the vertical, and we verified that the results were not sensitive to the moving average window size (*SI Appendix*, Fig. S2). We normalized the maximal voluntary force F_{max} of each trial by the maximal forces from all the trials of that subject to obtain a normalized force measure f_{max}. For each subject, we normalized the EMG recordings of each muscle with the moving average filtered maximal activity of the corresponding muscles. A PCSA-weighted average of the smoothed and normalized flexor EMG signals was used to find $EMG_{flexors}$.

Statistical methods. We report the mean $\pm$ SE of the change in f_{max} and $EMG_{flexors}$, calculated as the difference between the splinted and the free conditions, for the 2J and 1J splint. Additionally, descriptive statistics for F_{max} and $EMG_{flexors}$, and the change in normalized force f_{max} and $EMG_{flexors}$, are provided in *SI Appendix*, Tables S4 and S7.

Two one-way mixed-model type III ANOVAs using Satterthwaite's method tested the effect of splint (free, 1J, and 2J) and order of splint conditions on f_{max} and $EMG_{flexors}$, with subject as a random factor (*SI Appendix*, Table S5). Tukey contrasts for multiple comparisons of means were used, and the Bonferroni–Holm method was applied to find the adjusted *P* values (*SI Appendix*, Table S6). Two linear regressions, one for each splint type, modeled the relationship between the change in f_{max} and change in $EMG_{flexors}$ (*SI Appendix*, Table S8).

For 16 subjects in set C, we measured EMG_{EDC} along with EMG_{FDP} and EMG_{FDS}. An ANOVA tested the effect of finger condition on the ratio of EMG_{EDC} to $EMG_{flexors}$. Three ANOVAs tested the effect of finger condition on the EMG to normalized force ratios for FDS, FDP, and EDC. The Bonferroni–Holm method was applied on the multiple comparison of means to find the adjusted *P* values (*SI Appendix*, Tables S10 and S11). Using the difference between the linearly scaled splinted EMG_{EDC} for producing the same normalized maximal force as the free finger and the EMG_{EDC} for the free condition, we calculated the change in cocontraction of EDC (Δcc_{EDC}) between the splinted and the free condition (Fig. 4*B*). Three linear regressions tested the effect of change in cocontraction Δcc_{EDC} on the change in normalized fingertip force Δf_{max} (*SI Appendix*, Fig. S5 and Table S12), the effect of free finger's baseline force F_{free} (newtons) on the change in cocontraction Δcc_{EDC} (*SI Appendix*, Fig. S6 and Table S13), and the effect of free finger's baseline force F_{free} (newtons) on the change in fingertip force ΔF_{max} (newtons) (*SI Appendix*, Table S9), respectively.

We verified statistical assumptions of normality and equivariance (*SI Appendix*, Figs. S3, S4, and S7). Significance level for all statistical tests was a priori set to 0.05. RStudio (51) was used for the statistical tests. The complete dataset is provided as Datasets S1 and S2.

Data Availability. Text files with kinematic and kinetic data, and movies are included as supporting information.

ACKNOWLEDGMENTS. We thank P. Paoletti and anonymous referees for helpful comments. This work was supported, in part, by Wellcome Trust DBT Alliance Award 500158/Z/09/Z, NSF Grant CMMI-2046120, and Yale's Integrated Graduate Program in Physical and Engineering Biology (to M.V.), and the Pierre W. Hoge Foundation Fund, the Alpheus B. Stickney Scholarship Fund, and the National Centre for Biological Sciences (to N.S.).

1. J. R. Napier, The prehensile movements of the human hand. *J. Bone Joint Surg. Br.* **38-B**, 902–913 (1956).
2. M. W. Marzke, Precision grips, hand morphology, and tools. *Am. J. Phys. Anthropol.* **102**, 91–110 (1997).
3. F. A. Karakostis, G. Hotz, V. Tourloukis, K. Harvati, Evidence for precision grasping in Neandertal daily activities. *Sci. Adv.* **4**, eaat2369 (2018).
4. T. L. Kivell, Evidence in hand: Recent discoveries and the early evolution of human manual manipulation. *Philos. Trans. R. Soc. Lond. B Biol. Sci.* **370**, 20150105 (2015).
5. M. W. Marzke, Tool making, hand morphology and fossil hominins. *Philos. Trans. R. Soc. Lond. B Biol. Sci.* **368**, 20120414 (2013).
6. N. Hogan, S. P. Buerger, "Impedance and interaction control" in *Robotics and Automation Handbook*, T. R. Kurfess, Ed. (CRC, 2018), pp. 375–398.
7. R. M. Murray, Z. Li, S. S. Sastry, *A Mathematical Introduction to Robotic Manipulation* (CRC, 2017).
8. D. Whitney, Historical perspective and state of the art in robot force control. *Int. J. Robot. Res.* **6**, 3 (1987).
9. A. Bicchi, V. Kumar, "Robotic grasping and contact: A review" in *Proceedings 2000 ICRA. Millennium Conference. IEEE International Conference on Robotics and Automation* (Institute of Electrical and Electronics Engineers, 2000), **vol. 1**, pp. 348–353.
10. A. M. Okamura, N. Smaby, M. R. Cutkosky, "An overview of dexterous manipulation" in *Proceedings 2000 ICRA. Millennium Conference. IEEE International Conference on Robotics and Automation* (Institute of Electrical and Electronics Engineers, 2000), **vol. 1**, pp. 255–262.
11. D. Rancourt, N. Hogan, Stability in force-production tasks. *J. Mot. Behav.* **33**, 193–204 (2001).
12. N. E. Bunderson, T. J. Burkholder, L. H. Ting, Reduction of neuromuscular redundancy for postural force generation using an intrinsic stability criterion. *J. Biomech.* **41**, 1537–1544 (2008).
13. F. De Groote, J. L. Allen, L. H. Ting, Contribution of muscle short-range stiffness to initial changes in joint kinetics and kinematics during perturbations to standing balance: A simulation study. *J. Biomech.* **55**, 71–77 (2017).
14. A. Klimchik, D. Chablat, A. Pashkevich, Static stability of manipulator configuration: Influence of the external loading. *Eur. J. Mech. A Solids* **51**, 193–203 (2015).
15. H. Hanafusa, H. Asada, "A robot hand with elastic fingers and its application to assembly process" in IFAC Symposium *on Control Problems in Manufacturing Technology* (International Federation of Automatic Control, 1977), pp. 127–138.
16. M. T. Mason, Compliance and force control for computer controlled manipulators. *IEEE Trans. Syst. Man Cybern.* **11**, 418–432 (1981).
17. P. Akella, M. Cutkosky, "Manipulating with soft fingers: Modeling contacts and dynamics" in *1989 IEEE International Conference on Robotics and Automation* (Institute of Electrical and Electronics Engineers, 1989), pp. 764–769.
18. I. Kao, M. R. Cutkosky, R. S. Johansson, Robotic stiffness control and calibration as applied to human grasping tasks. *IEEE Trans. Robot. Autom.* **13**, 557–566 (1997).
19. E. Burdet, R. Osu, D. W. Franklin, T. E. Milner, M. Kawato, The central nervous system stabilizes unstable dynamics by learning optimal impedance. *Nature* **414**, 446–449 (2001).
20. L. P. Selen, D. W. Franklin, D. M. Wolpert, Impedance control reduces instability that arises from motor noise. *J. Neurosci.* **29**, 12606–12616 (2009).
21. R. J. Peterka, Sensorimotor integration in human postural control. *J. Neurophysiol.* **88**, 1097–1118 (2002).
22. K. Gellman, A. Ruina, A longer stance is more stable for a standing horse. bioRxiv [Preprint] (2021). https://doi.org/10.1101/2021.10.15.464610. Accessed 17 January 2022.
23. M. Venkadesan, F. J. Valero-Cuevas, Neural control of motion-to-force transitions with the fingertip. *J. Neurosci.* **28**, 1366–1373 (2008).
24. A. Schweizer, Biomechanical properties of the crimp grip position in rock climbers. *J. Biomech.* **34**, 217–223 (2001).
25. L. Vigouroux, F. Quaine, A. Labarre-Vila, F. Moutet, Estimation of finger muscle tendon tensions and pulley forces during specific sport-climbing grip techniques. *J. Biomech.* **39**, 2583–2592 (2006).
26. R. A. Marco, N. A. Sharkey, T. S. Smith, A. G. Zissimos, Pathomechanics of closed rupture of the flexor tendon pulleys in rock climbers. *J. Bone Joint Surg. Am.* **80**, 1012–1019 (1998).
27. M. W. Marzke, R. F. Marzke, Evolution of the human hand: Approaches to acquiring, analysing and interpreting the anatomical evidence. *J. Anat.* **197**, 121–140 (2000).
28. F. J. Valero-Cuevas, Predictive modulation of muscle coordination pattern magnitude scales fingertip force magnitude over the voluntary range. *J. Neurophysiol.* **83**, 1469–1479 (2000).
29. F. J. Valero-Cuevas, M. Venkadesan, E. Todorov, Structured variability of muscle activations supports the minimal intervention principle of motor control. *J. Neurophysiol.* **102**, 59–68 (2009).
30. R. S. Johansson, I. Birznieks, First spikes in ensembles of human tactile afferents code complex spatial fingertip events. *Nat. Neurosci.* **7**, 170–177 (2004).
31. P. M. Rack, D. R. Westbury, The short range stiffness of active mammalian muscle and its effect on mechanical properties. *J. Physiol.* **240**, 331–350 (1974).
32. L. Cui, E. J. Perreault, H. Maas, T. G. Sandercock, Modeling short-range stiffness of feline lower hindlimb muscles. *J. Biomech.* **41**, 1945–1952 (2008).
33. A. Z. Hajian, R. D. Howe, Identification of the mechanical impedance at the human finger tip. *J. Biomech. Eng.* **119**, 109–114 (1997).
34. F. J. Valero-Cuevas, F. E. Zajac, C. G. Burgar, Large index-fingertip forces are produced by subject-independent patterns of muscle excitation. *J. Biomech.* **31**, 693–703 (1998).
35. M. Venkadesan, F. J. Valero-Cuevas, Effects of neuromuscular lags on controlling contact transitions. *Philos. Trans. R. Soc. Lond. A Math. Phys. Eng. Sci.* **367**, 1163–1179 (2009).
36. K. D. Nguyen, N. Sharma, M. Venkadesan, Active viscoelasticity of sarcomeres. *Front. Robot. AI* **5**, 69 (2018).
37. X. Hu, D. Ludvig, W. M. Murray, E. J. Perreault, Using feedback control to reduce limb impedance during forceful contractions. *Sci. Rep.* **7**, 9317 (2017).
38. F. Doemges, P. M. Rack, Task-dependent changes in the response of human wrist joints to mechanical disturbance. *J. Physiol.* **447**, 575–585 (1992).
39. V. S. Chib, M. A. Krutky, K. M. Lynch, F. A. Mussa-Ivaldi, The separate neural control of hand movements and contact forces. *J. Neurosci.* **29**, 3939–3947 (2009).
40. W. Mugge, J. Schuurmans, A. C. Schouten, F. C. van der Helm, Sensory weighting of force and position feedback in human motor control tasks. *J. Neurosci.* **29**, 5476–5482 (2009).
41. M. Jeannerod, M. A. Arbib, G. Rizzolatti, H. Sakata, Grasping objects: The cortical mechanisms of visuomotor transformation. *Trends Neurosci.* **18**, 314–320 (1995).

42. M. Santello, J. F. Soechting, Gradual molding of the hand to object contours. *J. Neurophysiol.* **79**, 1307–1320 (1998).
43. M. A. Erdmann, M. T. Mason, An exploration of sensorless manipulation. *IEEE J. Robot. Autom.* **4**, 369–379 (1988).
44. M. Kazemi, J. S. Valois, J. A. Bagnell, N. Pollard, "Robust object grasping using force compliant motion primitives" in *Robotics: Science and Systems* (MIT Press, 2012), pp. 177–185.
45. E. J. Weiss, M. Flanders, Muscular and postural synergies of the human hand. *J. Neurophysiol.* **92**, 523–535 (2004).
46. M. Santello *et al.*, Towards a synergy framework across neuroscience and robotics: Lessons learned and open questions. Reply to comments on: "Hand synergies: Integration of robotics and neuroscience for understanding the control of biological and artificial hands." *Phys. Life Rev.* **17**, 54–60 (2016).
47. T. Takei, J. Confais, S. Tomatsu, T. Oya, K. Seki, Neural basis for hand muscle synergies in the primate spinal cord. *Proc. Natl. Acad. Sci. U.S.A.* **114**, 8643–8648 (2017).
48. M. Halaki, K. Ginn, "Normalization of EMG signals: To normalize or not to normalize and what to normalize to" in *Computational Intelligence in Electromyography Analysis–A Perspective on Current Applications and Future Challenges*, G. R. Naik, Ed. (InTech, 2012), pp. 175–194.
49. A. Burden, How should we normalize electromyograms obtained from healthy participants? What we have learned from over 25 years of research. *J. Electromyogr. Kinesiol.* **20**, 1023–1035 (2010).
50. B. Vanderborght *et al.*, Variable impedance actuators: A review. *Robot. Auton. Syst.* **61**, 1601–1614 (2013).
51. RStudio Team, RStudio: Integrated Development for R, Version 1.1.463 (RStudio, PBC, Boston, MA, 2016).